AGU PUBLICATIONS

JGR

Journal of Geophysical Research: Oceans

RESEARCH ARTICLE

10.1002/2016JC011773

Lagrangian pathways of upwelling in the Southern Ocean

Giuliana A. Viglione[1] and Andrew F. Thompson[1]

[1]Department of Environmental Science and Engineering, Division of Geological and Planetary Sciences, California Institute of Technology, Pasadena, California, USA

Key Points:
- Spatial and temporal variability of Southern Ocean upwelling is studied using virtual drifters
- Upwelling locations are highly constrained by topographic features
- Mean mixed layer residence times are found to be on the order of one month

Correspondence to:
G. A. Viglione,
gviglion@caltech.edu

Citation:
Viglione, G. A., and A. F. Thompson (2016), Lagrangian pathways of upwelling in the Southern Ocean, *J. Geophys. Res. Oceans*, *121*, 6295–6309, doi:10.1002/2016JC011773.

Received 4 MAR 2016
Accepted 4 AUG 2016
Accepted article online 8 AUG 2016
Published online 23 AUG 2016

Abstract The spatial and temporal variability of upwelling into the mixed layer in the Southern Ocean is studied using a 1/10° ocean general circulation model. Virtual drifters are released in a regularly spaced pattern across the Southern Ocean at depths of 250, 500, and 1000 m during both summer and winter months. The drifters are advected along isopycnals for a period of 4 years, unless they outcrop into the mixed layer, where lateral advection and a parameterization of vertical mixing are applied. The focus of this study is on the discrete exchange between the model mixed layer and the interior. Localization of interior-mixed layer exchange occurs downstream of major topographic features across the Indian and Pacific basins, creating "hotspots" of outcropping. Minimal outcropping occurs in the Atlantic basin, while 59% of drifters outcrop in the Pacific sector and in Drake Passage (the region from 140° W to 40° W), a disproportionately large amount even when considering the relative basin sizes. Due to spatial and temporal variations in mixed layer depth, the Lagrangian trajectories provide a statistical measure of mixed layer residence times. For each exchange into the mixed layer, the residence time has a Rayleigh distribution with a mean of 30 days; the cumulative residence time of the drifters is 261 ± 194 days, over a period of 4 years. These results suggest that certain oceanic gas concentrations, such as CO_2 and ^{14}C, will likely not reach equilibrium with the atmosphere before being resubducted.

1. Introduction

The Southern Ocean is a critical component of the global overturning circulation, especially due to its adiabatic pathways between the ocean interior and the mixed layer [*Marshall and Speer*, 2012]. The three-dimensional structure of the Southern Ocean, and in particular, the Antarctic Circumpolar Current (ACC), has also been suggested to have key controls on the overturning circulation and air-sea exchange [*Jones and Cessi*, 2016; *Tamsitt et al*., 2015; *Dufour et al*., 2015; *Thompson et al*., 2014; *Talley*, 2013; *Sallée et al*., 2012]. In particular, zonal structure is typically related to interactions with topographic features in the ACC. Furthermore, the ACC links the major ocean basins. Due to variations in stratification and water mass properties between the basins, the ACC encounters highly varying conditions along its northern boundary. Thus it is to be expected that the exposure of the lower overturning cell to the atmosphere, occurring through the outcropping of density surfaces into the surface mixed layer, also experiences zonal variations which can significantly impact climate via deep-ocean carbon storage and reventilation [*Marshall and Speer*, 2012; *Ferrari et al*., 2014].

The broad ventilation of deep waters and the subduction of surface and intermediate waters is one of the distinguishing features of the Southern Ocean. It is estimated that 15% of the surface area of the ocean, clustered around the Southern Ocean and the North Atlantic, is responsible for filling 85% of its interior volume [*Gebbie and Huybers*, 2011]. Whereas the location of subduction hot spots is critical for understanding interior property distributions, surface residence times must also be considered. Waters can only equilibrate with the atmosphere during the time they spend in the mixed layer. Once these waters are brought down into the deep ocean, their properties are conserved, since they are no longer subject to direct surface forcing. Although significant work has been done identifying regions and quantifying rates of subduction [e.g., *Broecker et al*., 1998; *Donners et al*., 2005; *Smethie and Fine*, 2001], there have been fewer such analyses of upwelling regions, with *Sallée et al*. [2010] providing a notable exception. Given the importance of water exchange in setting global climate, a thorough understanding of the mechanisms and time scales of both subduction and upwelling is critical to modeling the transport of dissolved gases and nutrients on a global scale.

Of particular importance is the uptake of carbon dioxide by the ocean. The ocean is able to mitigate the atmospheric effects of climate change by absorbing 25–30% of anthropogenically released carbon dioxide

annually [*Le Quéré et al*., 2009]. Several modeling studies have shown that oceanic sequestration of carbon is limited by the exchange of waters between the surface and interior oceans [*Sarmiento et al*., 1992; *Matear*, 2001; *Lévy et al*., 2013; *Bopp et al*., 2015], indicating that the Southern Ocean is the critical region where carbon-rich waters can be subducted and stored. Indeed, it has been found that more than 40% of anthropogenically released carbon enters the ocean south of 40° S [*Sallée et al*., 2012]. Thus, constraining the pathways of upwelling and subduction in the Southern Ocean is key to modeling and predicting future climate change.

The seasonally varying component of the mixed layer depth has been found to explain up to 88% of the variation in mixed layer depth around the Southern Ocean [*Sallée et al*., 2010]. However, this study was based on observations from Argo floats, which lack the resolution to distinguish mesoscale features. These smaller-scale patterns may also have a significant role to play in establishing variability of the mixed layer. In addition, there is a component of the variability that is due to spatial patterns of wind stress, buoyancy flux, and interactions with bottom topography. There are large zonal variations in mixed layer depths across the Southern Ocean, which have been thought to correspond in part to bathymetric features, as discussed by *Hägeli et al*. [2000] and shown in both our modeled mixed layer and observationally derived mixed layer fields (Figure 1). This influence is an indirect effect — the topography steers the circulation, which affects the slope of the outcropping isopycnals and thus, the mixed layer depth [*Sallée et al*., 2010]. Bathymetric features also significantly affect diapycnal and isopycnal diffusivities [*LaCasce et al*., 2014] and therefore, upward mixing. The spatially variable upward mixing affects the sites and rates of ventilation. The spatial pattern is also dictated by the variance in wind stress, heat and freshwater fluxes, and northward Ekman

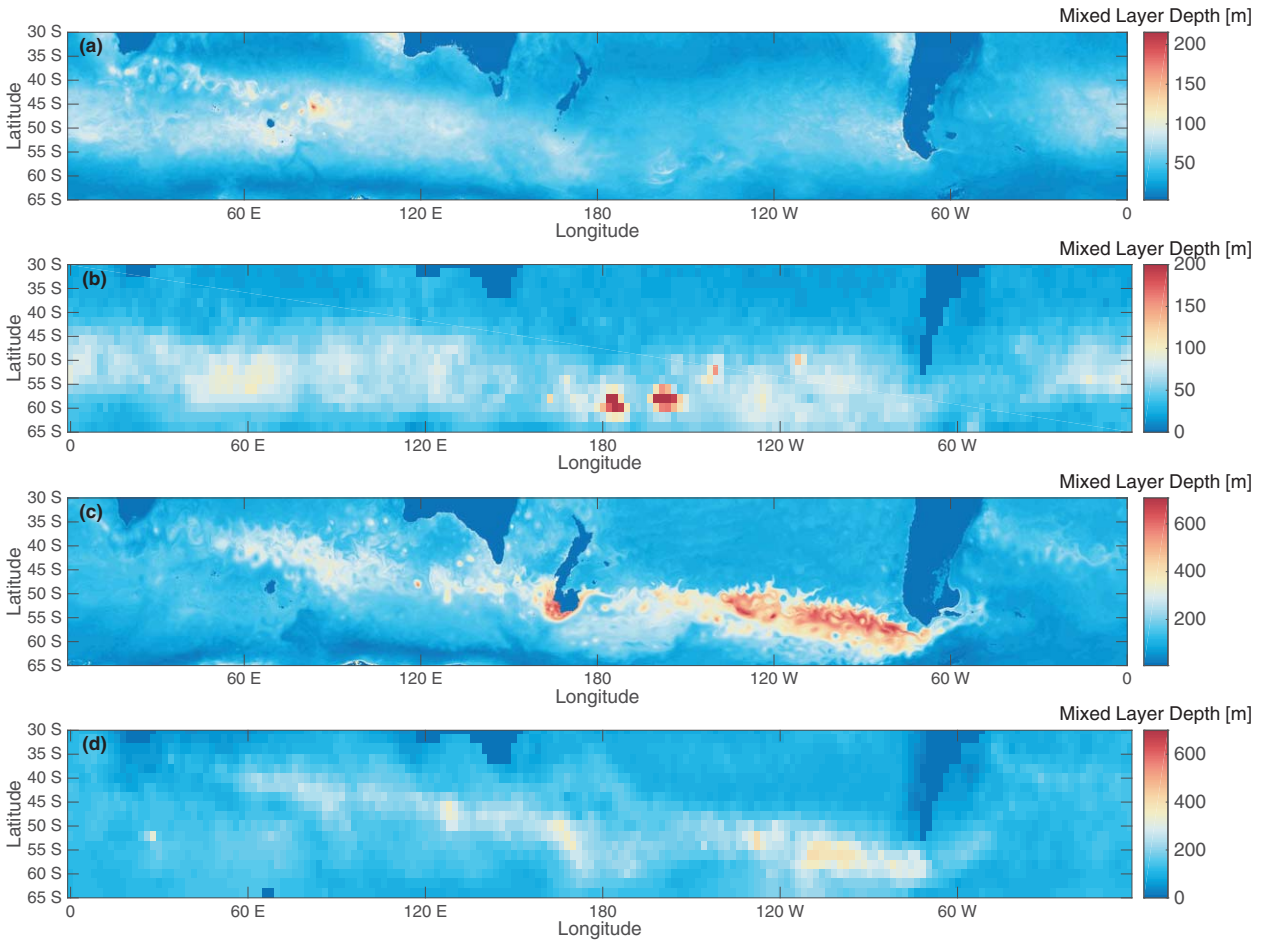

Figure 1. Seasonally averaged mixed layer depth for austral summer (DJF) from (a) OFES model output and (b) Argo float data and for austral winter (JJA) from (c) OFES output and (d) Argo data; note the change in color scale between plots. Notable features include mixed layer variability at mesoscales in both seasons and topographically localized mixed layer deepening in the JJA months.

transports of cold water. All of these processes, in addition to determining the mixed layer depth, are critical for setting the formation of mode waters in these regions [*Dong et al*., 2008].

Since the mixed layer depth, which is highly variable, is responsible for setting ventilation in the Southern Ocean, it follows that ventilation would also exhibit significant spatial patterns. *Sallée et al*. [2010] used a combination of satellite and *in situ* data alongside climatologies and parameterizations to estimate rates of ventilation around the Antarctic Circumpolar Current (ACC). They found highly localized regions of subduction and upwelling, and linked these to density classes corresponding to specific water masses such as Antarctic Intermediate Water (AAIW) and Subantarctic Mode Water (SAMW) at certain latitudes. Their conclusions are supported by data collected by Argo float profiles and analyzed for mixed layer depths around the Southern Ocean [*Dong et al*., 2008]. These authors find that the deepest mixed layers around the ocean occur in areas where the surface density (and thus, the density of the mixed layer) corresponds to that of SAMW, suggesting that these are regions where this mode water is formed. Mode waters also have a significant influence on global climate, as they can "store" climate anomalies from 1 year to the next by acting as an upper-ocean reservoir for anomalous heat, nutrients, and carbon dioxide [*Kwon et al*., 2015]. Our focus here allows us to examine the interior sources of what will eventually be subducted as mode waters.

In this study, high-resolution ocean model output is paired with an isopycnal advection scheme and used to identify Lagrangian pathways of Southern Ocean transport and localized regions of significant upwelling activity. Similar approaches have been used to study oceanic currents since the mid-1990s [*Davis et al*., 1996], but increased computational power over the past two decades has meant that results from this type of study have resolved more structure. Similar analyses to the study performed here have been used to examine water export from Drake Passage [*Friocourt et al*., 2005], abyssal export of Antarctic Bottom Water [*van Sebille et al*., 2013], and transport pathways along the western Antarctic Peninsula [*Piñones et al*., 2011], among other phenomena. Several studies also compare simulated drifter trajectories to pathways mapped via drifters and/or floats [e.g., *Kwon et al*., 2015; *Gary et al*., 2012; *van Sebille et al*., 2009]. The advantages of a Lagrangian study are that it allows an examination of the pathways connecting intermediate waters to the surface ocean and an exploration of the interconnectivity of the ocean basins in a three-dimensional sense.

The following section, section 2, describes the model output and the Lagrangian trajectory algorithm. Section 3 discusses the results of the simulations. Section 4 provides an interpretation of the findings of the study and examines its limitations, while section 5 summarizes the paper.

2. Methods

2.1. Description of the OFES Model

We examine the Lagrangian pathways of interior-mixed layer exchange and surface residence times through the use of an eddy-resolving numerical simulation, which allows us to capture temporal/spatial scales and durations that are challenging for most observing systems, e.g., ships or Argo floats. Our approach is to use an eddy-resolving model of the Southern Ocean in order to accurately portray these mesoscale motions. Ocean Global Climate Model for the Earth Simulator (OFES) is a 1/10° model with 54 variably spaced levels and realistic bathymetry [*Masumoto et al*., 2004]. OFES is based on GFDL/NOAA's Modular Ocean Model version 3 (MOM3), with bathymetry based on the OCCAM project at Southampton Oceanography Centre. Although the OFES model goes to 75° S, output was only loaded to 65° S for computational efficiency; since less than 7% of outcropping occurred south of 60° S, this choice is unlikely to have skewed the results of this study in any meaningful way.

OFES provides daily snapshots of temperature, salinity, and three-dimensional velocity fields for a period of 8 years (1990–1997) following a 50 year spin-up using monthly climatological forcing. There is no difference in surface forcing across the different years, but internal variability exists. Thus, the climatological forcing better allows an estimate of the influence of internal eddy variability on outcropping and was therefore chosen over the interannual forcing used by *van Sebille et al*. [2012]. This study loaded model output every third day and interpolated between the snapshots using a spline interpolation scheme to provide the fields at each timestep. Previous work with this model had confirmed that high-frequency dynamics of the region were not aliased by sub-sampling in this manner [*Thompson and Richards*, 2011].

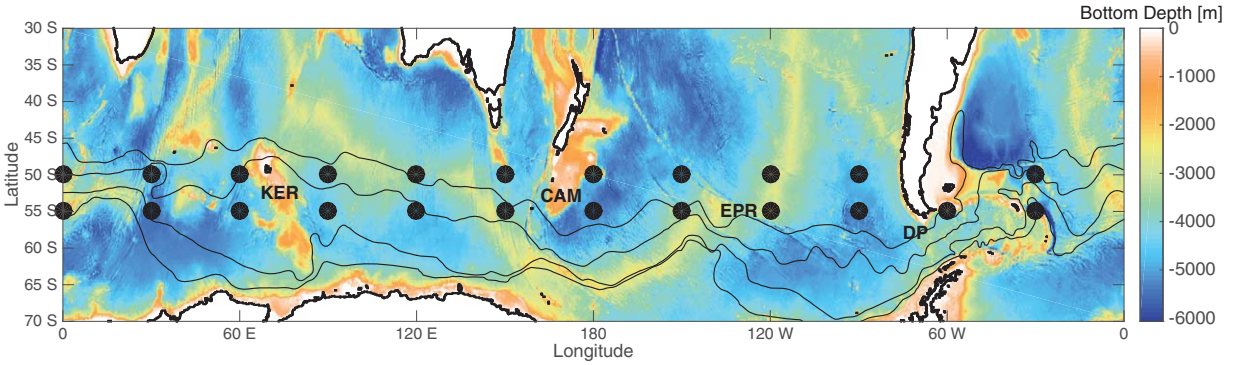

Figure 2. Bathymetry of the Southern Ocean in the OFES model; black circles represent the deployment zones of the virtual drifters. Each deployment occurred in a 2° by 2° box. For each point shown, a total of 6 deployments were performed: at depths of approximately 250, 500, and 1000 m, and at starting dates of both 1 January and 1 July. See details in section 2. Black lines denote the climatological mean fronts of the Southern Ocean as given by *Orsi et al.* [1995]. From top to bottom: the Subantarctic Front, the Polar Front, the Southern ACC Front, and the Southern Boundary of the ACC. Labels denote the major bathymetric features discussed in this work: Kerguelen Plateau, KER; Campbell Plateau, CAM; East Pacific Rise, EPR; and Drake Passage, DP.

2.2. Description of Deployments and the Advection Scheme

Virtual drifters were released in the OFES model at 23 different sites in the ACC; at each of these sites, 1000 drifters were released at each of three different depths and on two different starting dates. Deployments were evenly spaced at 30° longitude increments at both 50° S and 55° S, with no deployments at 50° S, 60° W due to the shallow bathymetry at this location (shown in Figure 2). For each deployment site, initial drifter positions were randomly distributed within a 2°-by-2° box centered at the given coordinates. At each location, deployments were performed on each of three isopycnal surfaces. The chosen potential density surfaces were not necessarily the same at each deployment site, but rather, were selected to coincide with approximate initial depths of 250, 500, and 1000 m.

The drifters were initialized on either 1 January or 1 July and advected forward for a period of 4 years using a time step of 2 h. The drifter trajectories are constrained by design to be adiabatic in the interior; no subgrid scale diffusion was added. Thus, at each time step, the two-dimensional horizontal velocity field is interpolated on to the density surface of each drifter position and used to update the horizontal position, while maintaining the trajectory on a density surface determines the vertical displacement. While diapycnal mixing is small throughout most of the Southern Ocean, larger diapycnal velocities can occur near topographic features [*Sheen et al.*, 2013]. However, as shown below, mixed layer outcropping events are qualitatively similar at all deployment depths, e.g., outcropping sites are not strongly dependent on particular isopycnals. Thus, our assumption of an adiabatic interior is unlikely to change the spatial characteristics of the outcropping events. A sample set of trajectories and a depth-time plot for a single deployment are shown in Figure 3. Over the 4 year advection period, drifters, deployed at 250 m, occupy roughly half the zonal extent of the ACC. For this particular deployment, the vertical dispersion of the drifters increases abruptly after day 423, which coincides with the passage of the drifters' mean position over and around Kerguelen Plateau.

The assumption of isopycnal motion was relaxed when drifters cross into the mixed layer. The mixed layer was defined by a density difference criterion of $\rho = 0.03$ kg/m^3 from the density at 10 m depth, following *de Boyer Montégut et al.* [2004]. Once drifters crossed into the mixed layer, it is assumed that the turbulent mixing dominates the vertical displacement of the drifter. Thus we applied a random walk in the vertical with a maximum displacement of 20 m per time step, similar to the method employed by *van Sebille et al.* [2013] and consistent with an average diapycnal diffusivity of 139×10^{-4} m^2 s^{-1} acting over the 2 h time step. This mixed layer diffusivity is consistent with values previously determined by *McPhee and Martinson* [1994] and *Large et al.* [1994]. In the mixed layer, the horizontal displacements were determined by advection by the local horizontal velocities. The drifter advection algorithm avoided vertical advection out of the mixed layer. If the random walk placed a drifter above the ocean surface, it was restored to a depth of 5.5 m. If the drifter was displaced out of the bottom of the mixed layer, it was placed 0.5 m above the base of the mixed layer. A sensitivity study was performed on this parameter; there was no change in outcropping frequency or pattern for placement between 0.1 and 5 m above the base of the mixed layer. This meant that the drifters

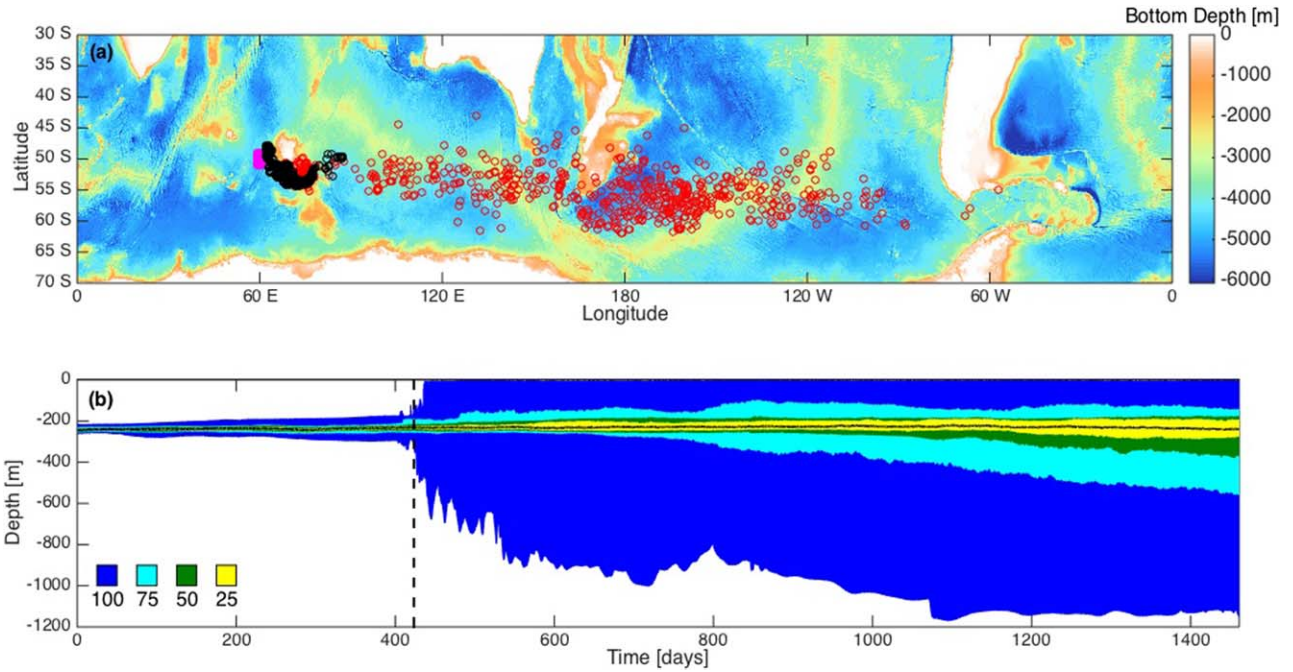

Figure 3. Sample diagnostics from a single deployment, centered at 50° S, 60° E and a depth of 250 m; the deployment date was 1 July. (a) Trajectories of individual drifters over a 4 year period indicating deployment locations (magenta circles) and ending locations (red circles). (b) Vertical distribution of the drifters, as given by the envelope containing 25% (yellow), 50% (green), 75% (cyan) and 100% (blue) of the drifters. The thick black curve gives the mean depth of all drifters. The dashed line at day 423 corresponds to most drifters reaching the Kerguelen Plateau and corresponds to the black circles in Figure 3a.

could only leave the mixed layer by horizontal advection across lateral mixed layer gradients, or by a shoaling of the mixed layer above their position. This minimizes rapid, high-frequency exchange across the base of the mixed layer, but physically represents reduced mixing turbulence and a stronger stratification at the base of the mixed layer.

When drifters exited the mixed layer, they were not required to return to the density surface they occupied prior to entering the mixed layer. The new density surface at which they crossed the base of the mixed layer back into the interior was recorded and subsequent advection in the interior followed this new surface. Thus, changes in density between upwelling and subduction provide an indication of the sense of water mass modification in the mixed layer. Throughout each deployment, time series were recorded of latitude, longitude, depth, and density of each drifter, as well as the mixed layer depth at the drifter position and a bianary diagnostic labelling whether the virtual drifter was in or out of the mixed layer.

3. Results

An instance of outcropping was defined as a time at which a drifter was in the mixed layer and had not been in the mixed layer at the time step immediately prior. Thus for each drifter, we can obtain the latitudes and longitudes of each instance of outcropping throughout the simulation. This approach is similar to the Lagrangian analysis of front-crossing events in *Thompson and Sallée* [2012]. These instances of outcropping are binned into 1°-by-1° boxes (Figure 4). Each instance of outcropping is counted, regardless of prior instances of outcrop. In order to highlight the contrast between regions of high outcropping and those of low outcropping, the number of drifters per box is displayed on a logarithmic color scale. The spatial patterns and indeed, the intensity (defined by the number of outcropping drifters), of outcropping events are qualitatively similar between the set of drifters deployed in austral summer and those deployed in austral winter, with the root mean squared difference between the boxes only 13 instances of outcropping over the course of the simulation. This similarity can be attributed to the tendency of drifters to primarily outcrop in winter regardless of season of deployment, which will be discussed in detail later on. Relatively little outcropping occurs in the Atlantic and Indian basins, with upwelling predominately happening in the Pacific

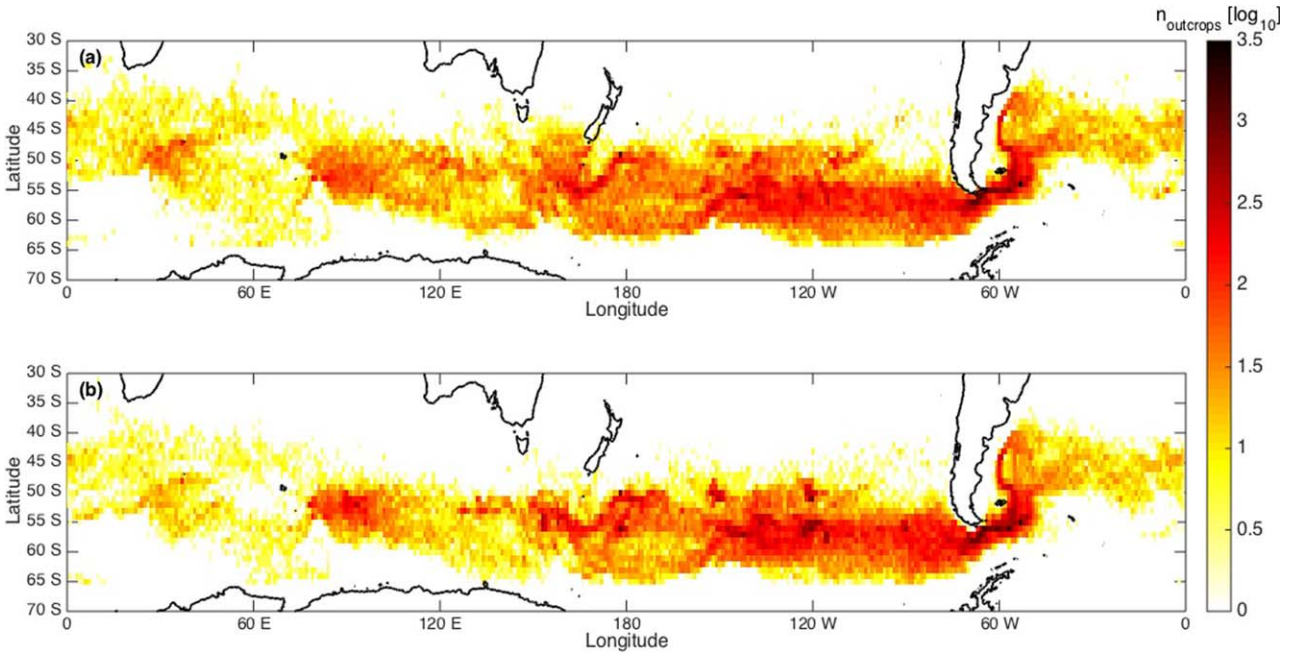

Figure 4. Heat map showing all outcropping locations (logarithmic scale) across the 138 deployments (138,000 trajectories) for the (a) 1 January deployments and (b) 1 July deployments. Outcropping events were binned into 1°-by-1° boxes and summed over the entire duration of the simulations. Increased upwelling occurs downstream of significant bathymetric features: Kerguelen Plateau, Campbell Plateau, the East Pacific Rise, and within and downstream of Drake Passage.

sector. 59% of outcropping events occur in the ACC between 140° W and 40° W. Furthermore, outcropping appears to be concentrated in distinct regions within the sector, rather than occurring uniformly throughout the ocean; 23% of outcropping events occur over the 4% of longitudes encompassing Drake Passage (Figure 4).

The spatial patterns of upwelling are similar between the drifters deployed at 250 m and 500 m, as both show strong signals of upwelling in Drake Passage and throughout the Pacific (Figure 5). However, there is notably less upwelling from the 500 m depth in the Indian basin; in addition, although the enhanced outcropping zones still exist, the strength of these hotspots in comparison to the rest of the basins is reduced when examining the set of drifters deployed at 500 m. Outcropping events are an order of magnitude or more smaller for those drifters deployed at 1000 m due mainly to the limited length of integration; the majority of these outcropping events is in the eastern Pacific sector of the ACC and within Drake Passage. From top to bottom, these plots show outcropping for drifters deployed at (a) 250 m, (b) 500 m, and (c) 1000 m. The colorbars for Figures 5a and 5b are the same logarithmic scale, while the colorbar shifts for Figure 5c due to the greatly reduced instances of outcropping.

Distinct regions of the ocean are seen to contain most instances of outcropping (Figures 4 and 5). In order to determine what set these locations apart from other sites in the ocean, outcropping "hotspots" were defined as those 1°-by-1° grid boxes in which there had been 600 or more instances of outcropping across all simulations. 73 grid boxes were found to meet this criterion, with 17% of outcropping events occurring in only 0.6% of grid boxes. Several further methods of analysis were aimed at determining the differences between these regions and the remainder of the ocean. For all depths studied, the distribution of densities outcropping in the hotspot regions was narrower than the density distribution of all outcropping events (Figure 6), even though outcropping hotspots are found in the Pacific and Indian sectors as well as Drake Passage. Figures 6a–6c show the frequencies of density at outcrop by starting depth—250 m, 500 m, and 1000 m, respectively. The histograms show the frequency of all outcropping, the frequency of outcropping in hotspots and the initial deployment density distributions. Note that drifters may outcrop in density classes lighter than the deployment density range (as long as it is not the first outcropping event in the trajectory) due to modification in the mixed layer. The spatial pattern of the outcropping of these density classes is qualitatively similar to those shown in *Sallée et al.* [2010, Figure 10].

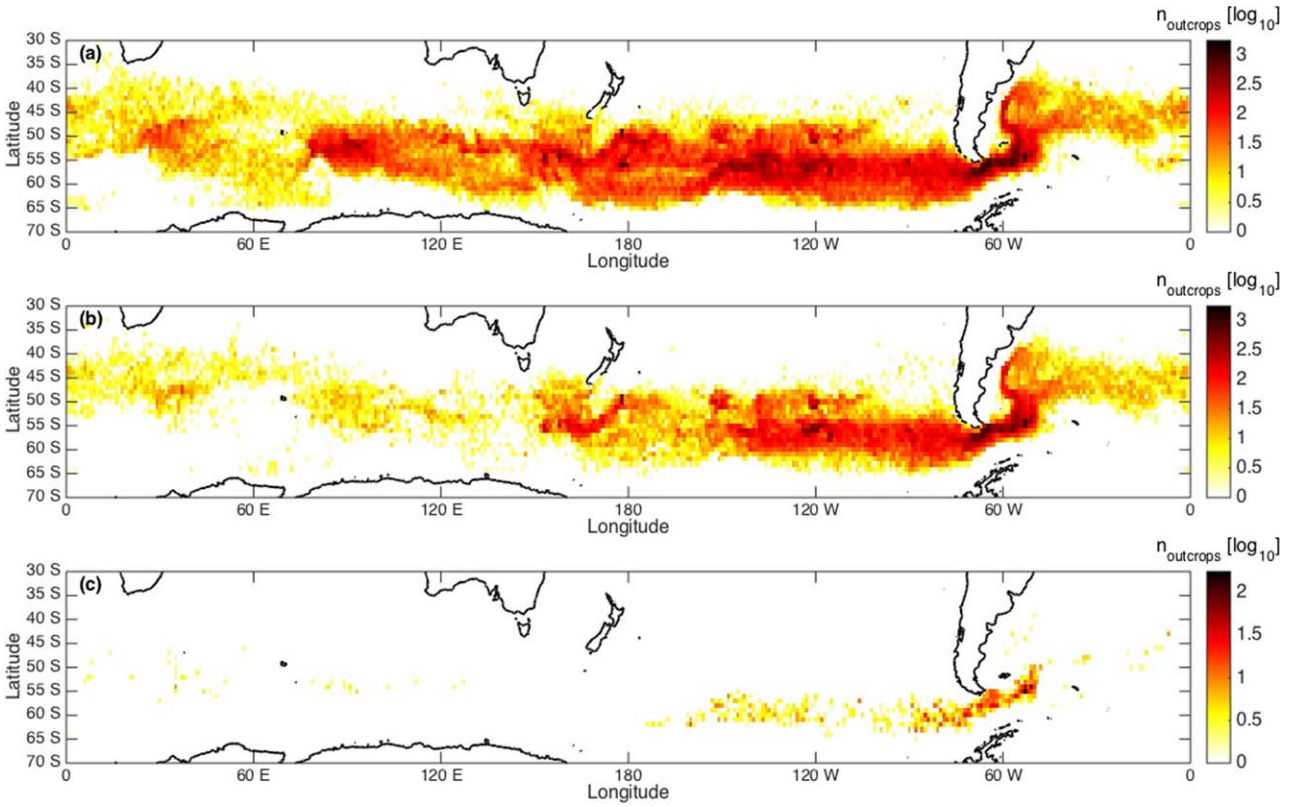

Figure 5. As in Figure 4: a heat map of outcropping zones for drifters deployed at (a) 250 m, (b) 500 m, and (c) 1000 m depths.

Only drifters originating from certain regions outcrop during this 4 year period. Less than 5% of outcropping drifters were sourced from each longitude between 30° E and 60° W, a feature that is even more striking when considering only drifters that first outcropped in a hotspot region. In this case, each of these longitudes contributes $< 1\%$ of outcropping drifters (Figure 7). Across all outcropping drifters, the percentages outcropping starting at the remaining latitudes were roughly equal, with only the deployments at

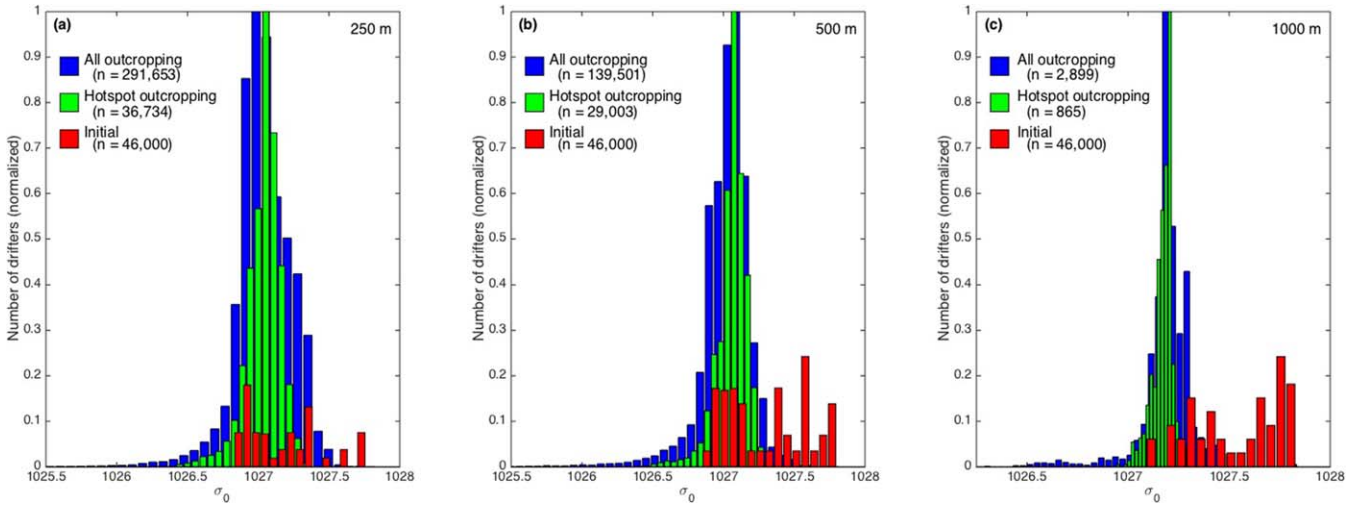

Figure 6. Frequency of outcropping as a function of density classes for (a) 250 m, (b) 500 m, and (c) 1000 m deployments. The density class gives the drifter's isopycnal at the time of outcrop; this is calculated for all drifters (blue) and those drifters that outcrop at hotspot locations (green). The red values show initial deployment densities. For easier comparison, the blue and red histograms are normalized to the maximum of the blue; the green was normalized to its maximum. The total number of drifters in each category is listed on each plot. In Figure 6c, the initial density distribution (red) was reduced by a factor of 40.

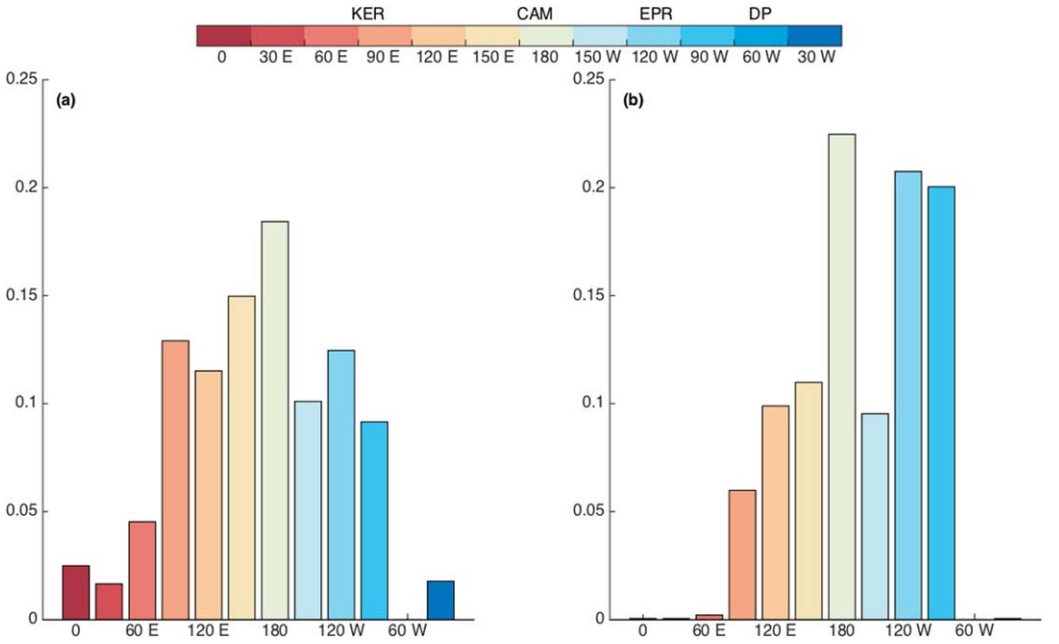

Figure 7. Summary of initiation longitude for (a) all outcropping drifters for (b) drifters outcropping in hotspot zones. Labels above the colorbar indicate approximate positions of major bathymetric features: Kerguelen Plateau, KER, Campbell Plateau, CAM, East Pacific Rise, EPR, and Drake Passage, DP.

150° E and 180° showing significantly higher instances than the other longitudes. However, in the case where only outcrops in hotspot zones were considered, significantly more drifters outcrop at 180°, 120° W, and 90° W, with these three longitudes alone responsible for nearly 2/3 of the outcropping drifters.

There is also a spatial pattern to the average age at which drifters outcrop, with young drifters upwelling in the West Indian and Pacific sectors and older drifters outcropping in Drake Passage and the Atlantic. Drifters upwelling on the southern flank of the ACC also tended to be significantly older than the drifters upwelling further north; note that the southernmost outcropping positions are located further away from the

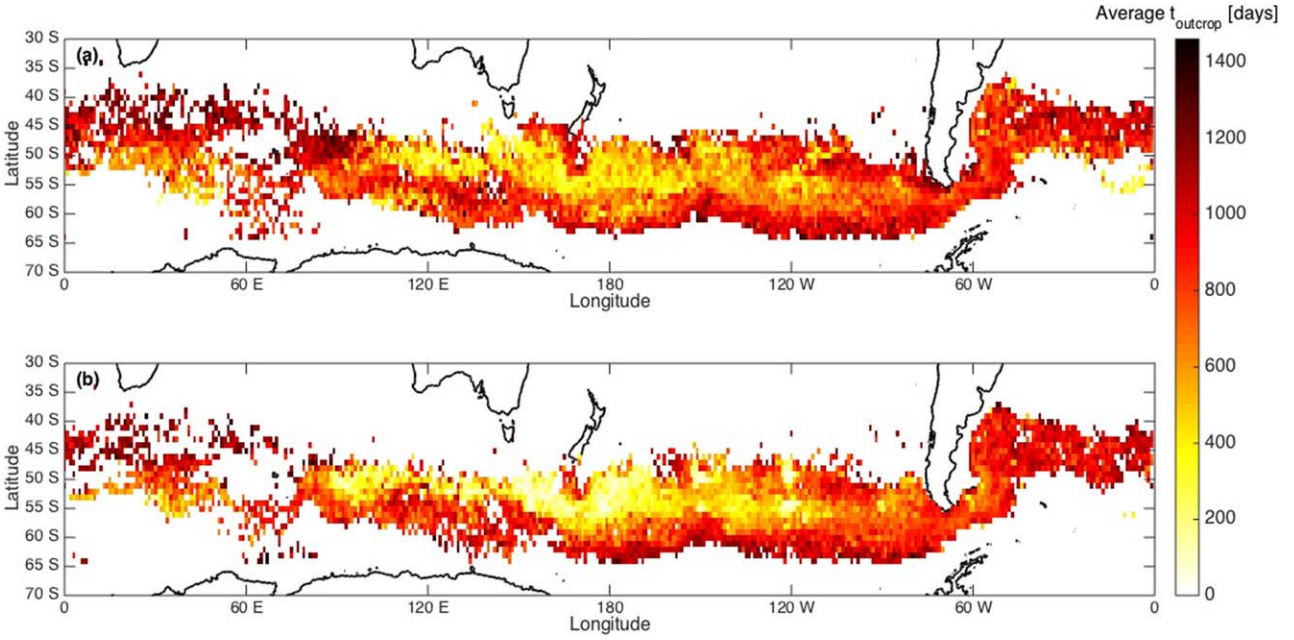

Figure 8. Average time (days) to first outcrop since deployment dates of (a) 1 January and (b) 1 July across the Southern Ocean. Drifters from all depths are included.

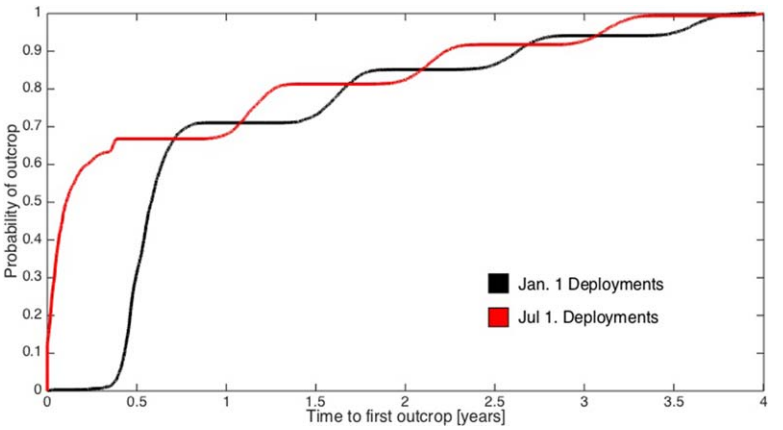

Figure 9. Cumulative distribution functions (CDF) depicting the time to first outcrop for each drifter that outcropped at least once during the simulation. The black curve shows the CDF for drifters that were deployed in January; the red curve shows the CDF for drifters deployed in July.

deployment latitudes. On average, it takes less time for drifters deployed in July to outcrop, as compared to the January deployments. This feature is especially distinct in the Indo-Pacific sector (Figure 8), emphasizing the importance of the seasonal cycle of mixed layer depths in setting outcropping locations. This figure displays the average time, measured from the deployment date, for a drifter to outcrop for each 1° by 1° grid box. This represents the mean time to outcrop averaged over all drifters outcropping in a particular box. Only boxes in which at least 5 drifters outcropped were included in the map. The two plots show drifters deployed on (a) 1 January and (b) 1 July. The patterns in Figure 8 are consistent with the data in Figure 7, which show the source region being spatially localized; thus the difference in time to outcropping sites reflects the advection period.

The majority of drifters outcrop within the first year. Roughly 2/3 of the drifters deployed on a given date outcrop within 0.4 years of the corresponding austral winter season, with the remaining drifters outcropping at a slower and slower rate throughout the remainder of the simulation. This timing is dominated by the seasonal variations of the mixed layer depth with most outcropping events occurring in winter. Thus July deployments are rapidly entrained into the mixed layer, while January deployments experience a $\sim$6 month advection period before outcropping becomes intense (Figure 9). This seasonality of outcropping persists throughout the 4 year deployment and can be seen through the distinct step-like shape of the curves in Figure 9.

The season in which drifters are deployed also has little effect on the patterns of outcropping as a function of mixed layer depth, with the majority of drifters doing so in regions where the mixed layer is between 50 and 200 m deep. However, when outcropping hotspots are considered, this peak occurs over a narrower range, between 100 and 200 m depth (Figure 10). Here, all outcropping instances are shown in Figure 10a, while in Figure 10b, only drifters outcropping in hotspot regions are taken into account. Each plot shows three lines: one which represents 1 January deployments (red), one which represents 1 July deployments (green), and one which represents mixed layer depths over an annual cycle (black dashed). By comparing the two plots, it is apparent that there is a sharper peak in the mixed layer depths at outcropping hotspot regions and that this peak occurs at shallower depths than the corresponding peak when the full domain is considered. This suggests that mixed layer depth alone is not able to explain the phenomenon of these outcropping hotspots.

After 4 years of forward advection, only a small subset of drifters spend more than 2 cumulative years in the mixed layer, and virtually no drifters persist longer than 3 years of deployment. On average, if a drifter crosses into the mixed layer at least once during its deployment, it will spend a period of 261 days in the mixed layer (Figure 11). The four lines in Figure 11 correspond to snapshots taken at the end of each year of deployment, such that the blue curve contains data from the first year, the red curve contains data from the first 2 years, and so on. The mean cumulative residence time increases as each year passes, as signified by the circles on the x-axis of Figure 11, which show the mean residence time at the end of each year of the

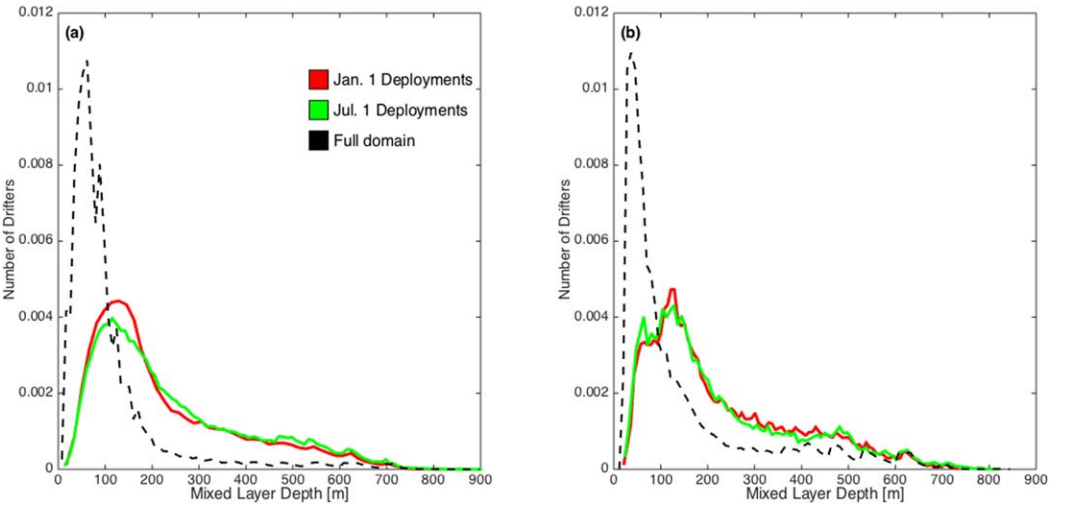

Figure 10. Probability distribution functions showing the mixed layer depth at a drifter's point of outcrop for (a) all outcropping drifters and (b) for drifters outcropping in hotspots. The outcropping events are normalized such that the area under the curve sums to 1 and the *x* axis gives the mixed layer depth in meters. The histograms are split by deployment date, with 1 January deployments in red and 1 July deployments in green. Mixed layer depths over 1 year across the domain (from 45° S to 65° S) are given by the dashed line in Figure 10a, while mixed layer depths over the same 1 year period at the hotspots are given by the dashed line in Figure 10b.

simulation. The inset figure shows the mean time spent in the mixed layer by an outcropping drifter as a function of simulation time, with the magenta line providing a reference scenario in which all drifters spend all their time in the mixed layer. A fit to this curve shows that outcropping drifters spend, on average, 20% of their time in the mixed layer, a result that is robust regardless of season of deployment. Initial depth of deployment also has a small effect on this result, with drifters deployed at 250 m spending 22% and those deployed at 500 m spending 17% of their time in the mixed layer.

Throughout the 4 year deployment, a greater number of drifters are gaining density during their residence in the mixed layer, but the amount of density modification for drifters losing density is much higher than it

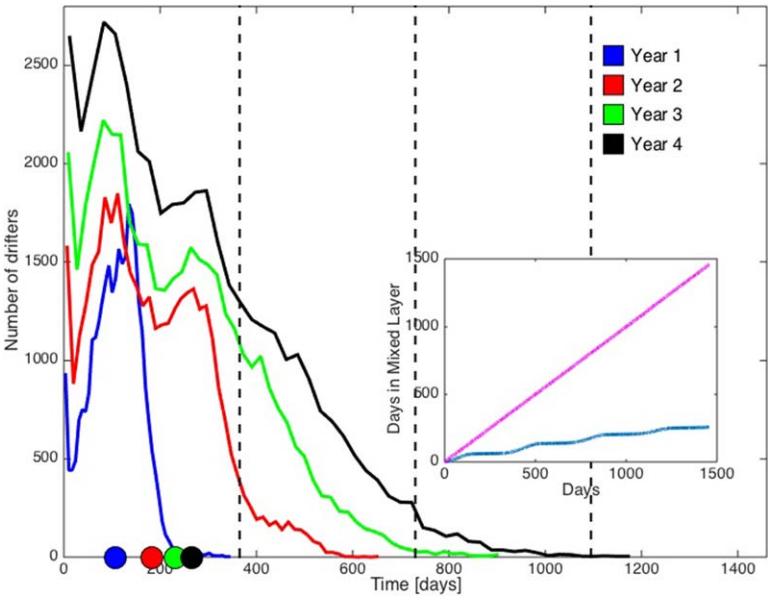

Figure 11. Cumulative mixed layer residence time for all drifters that outcrop at least once. The blue, red, green, and black lines respectively represent the first, second, third, and fourth years of deployment (inclusive). The dashed vertical lines delineate the years since deployment. The circles along the x-axis denote the mean residence times for each year of the simulation. Inset: Days of simulation versus the mean time spent in the mixed layer. The magenta line represents the scenario that all outcropping drifters stay in the mixed layer for the duration of the simulation. The blue curve is the mean over the July deployments.

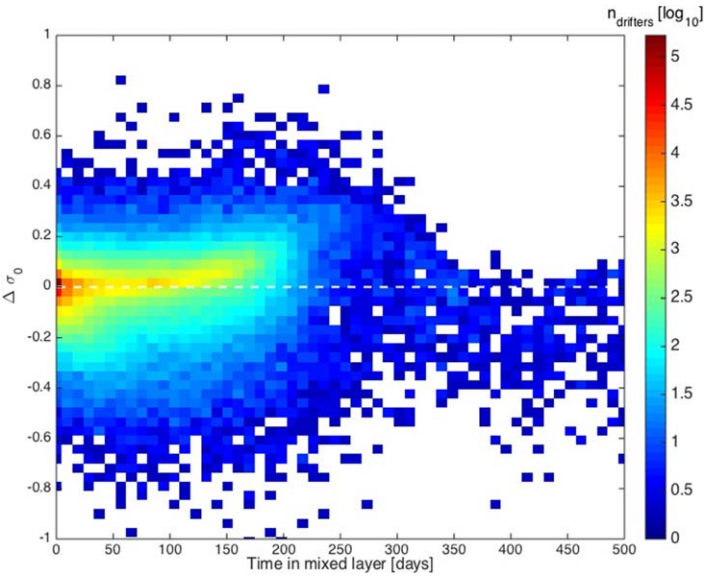

Figure 12. Two-dimensional histogram depicting change in density between drifters entering and exiting the mixed layer. On the *x* axis is the number of consecutive days spent in the mixed layer. The *y* axis shows the change in potential density, σ_0 (kg m^{-3}). The colorbar is on a logarithmic scale. White line indicates zero density modification.

is for drifters that gain density. In fact, the average amount of density gain in the mixed layer is $+0.22$ kg/m^3, while the average amount of density loss is -0.47 kg/m^3. This result suggests that there is a net densification of water in the mixed layer in the study region. This is corroborated by the results of *Iudicone et al.* [2008], who showed net downwelling over the bulk of the density classes examined in this study. Additionally, the amount of time spent in the mixed layer seems to have a fairly small effect on the amount of density modification that occurs (Figure 12), likely reflecting both the nonlinearities produced by the mixed layer and buoyancy flux variability and the way in which the mixed layer has been parameterized in this study. In this figure, each instance of outcropping was counted separately, even if a drifter outcropped multiple times.

4. Discussion

4.1. Localization of Outcropping

As noted in section 3, there is significant spatial variability in outcropping sites across the Southern Ocean, a trend that persists regardless of the season in which drifters were deployed or their initial depths. While few drifters outcrop in the Atlantic and Indian basins, significant outcropping occurs in the Pacific, a result that is evident even when considering the relative sizes of the ocean basins. Examining smaller scales, the outcropping is predominantly constrained to specific, highly localized regions of the ocean, which appear to be correlated with major bathymetric features of the ocean. "Hotspots" of upwelling can be seen near Kerguelen and Campbell Plateaus, in the lee of the East Pacific Rise, and throughout Drake Passage, all regions in which there are abrupt changes in topography over relatively short horizontal distances.

As shown by Figure 1, deep mixed layers ($>$ 500 m) are seasonally found in the lee of major bathymetric features of the Southern Ocean. This may lead to the conclusion that topographic deepening of mixed layers is responsible for enhanced entrainment of waters and thus, increased outcropping frequency in the lee of these major plateaus and ridges. It is important to note that the modeled mixed layer depths show significant ($>$ 50 m) deviation from the observed mixed layer depths over much of the Southern Ocean, especially when attempting to resolve the deep wintertime mixed layers of the Indian basin. However, as shown in Figure 10, the majority of outcropping is occurring into shallower mixed layers on the order of 100–200m. This suggests that there may be another mechanism responsible for setting the locations of the hotspot outcropping zones, such as deflection of isopycnals upward over significant bathymetry, causing water masses to rise in the water column and then advect across lateral mixed layer depth gradients downstream of these features, as discussed by *Sallée et al.* [2010].

4.2. Buoyancy Forcing and Variability

As water masses are exposed to the surface mixed layer, surface buoyancy forcing may modify the surface layer such that subsequent subduction need not occur on the same isopycnal on which the water upwelled. This diabatic transport in the mixed layer is a major component of the water mass modifications in the Southern Ocean. It has been proposed that both limbs of the overturning circulation, e.g., waters becoming

both more and less buoyant at the surface, outcrop in the ACC [*Marshall and Speer*, 2012], although we note that the largest sources of densification are likely to occur very close to the Antarctic coast [*Rintoul*, 2013; *Naveira Garabato et al*., 2016]. Previous work has shown the importance of buoyancy fluxes within the ACC on the global overturning circulation [*Weijer et al*., 2002; *Marshall and Speer*, 2012]. A direct diagnosis of the of the water mass transformation, as completed in *Bishop et al*. [2016] and *Newsom et al*. [2016], is beyond the scope of this study, but would be reflected in the mixed-layer drifter tendencies if the model is in a statistically steady state.

The zonal structure of buoyancy forcing in the Southern Ocean has been the focus of recent work emphasizing its impact on the global OC [*Cerovečki et al*., 2011; *Tamsitt et al*., 2015; *Thompson et al*., 2015]. As seen in Figures 4 and 5 and discussed in section 4.1, strong spatial patterns of upwelling exist across the Southern Ocean; this will lead to similarly variable patterns of buoyancy fluxes, since the Southern Ocean is responsible for the spatial variability of air-sea buoyancy exchange, as shown in *Tamsitt et al*. [2015]. Indeed, the zonal structure in surface buoyancy flux shown by that work reflects the locations of the outcropping hotspots identified in this study. However, attempts at calculating the intensity of the overturning circulation, as mediated by surface buoyancy forcing, typically rely on climatological estimates of the surface buoyancy distribution, surface flux, and mixed layer depth, e.g., *Marshall and Radko* [2003]. These terms combine in a nonlinear expression for the overturning streamfunction. However, since all three of these terms are time-dependent, it is not clear that time-averaged or climatological values of these properties will provide accurate estimates of the overturning streamfunction. Our results show all of these properties exhibit intermittency in both space and time. The temporal correlation of these different properties and their impact on overturning rates remain relatively unexplored.

4.3. Mixed Layer Residence Times

One of the notable results of this study, as seen in Figure 11, is the relatively short residence time experienced by waters in the mixed layer in the Southern Ocean. During the July deployment, roughly two-thirds of the drifters outcrop in the first three months following deployment. Yet, on average, the drifters spend less than half a year in the mixed layer. The combination of the spatial heterogeneity and the seasonal cycle of the mixed layer causes a long-term residence time, e.g., over a seasonal cycle, to be rare. The implications of this short residence time is that the ability of a Lagrangian water mass to equilibrate gases concentrations via air-sea exchange will undergo a seasonal cycle with reduced opportunities to exchange properties in the biologically productive summer months. Previous studies have quantified the air-sea equilibration timescale for carbon dioxide as ranging from 6 to 24 months; the high end of this range is typically associated with the Southern Ocean south of Australia and New Zealand [*Jones et al*., 2014]. Combined with the inset of Figure 11, this suggests that over large swaths of the Southern Ocean, complete equilibration of carbon dioxide with the atmosphere may take 5–10 years. If this is shorter than the timescale of subduction of a given parcel into the ocean interior, full equilibration may be highly limited around the Southern Ocean.

Another implication of the seasonality drifters experience in the mixed layer is that the cumulative residence time is also lowered. Again referring to Figure 11, the cumulative residence times approximate a Rayleigh distribution. Since a Rayleigh distribution is found in cases where two noncorrelated, normally-distributed variables combine to produce a third quantity. In this case, the mixed layer depth and the vertical position/trajectory of the drifters influence the residence time of the drifters in the mixed layer. The vertical positions are close to a normal distribution given the treatment of particles in the mixed layer; the mixed layer depths can be crudely approximated by a normal distribution. Thus, as a rudimentary fit, the Rayleigh distribution is appropriate, although this could certainly be the subject of further examination in future work. This figure also demonstrates that over the course of the 4 year simulation, no drifters are able to remain in the mixed layer for close to the entire length of the simulation. In fact, few drifters even spend 3 cumulative years in the mixed layer. This, too, affects the extent to which waters can equilibrate carbon dioxide and other properties with the atmosphere. From Figure 12, there is no apparent correlation between mixed layer residence time and the magnitude of density modification, as measured by the difference in isopycnal upon entering and exiting the mixed layer. This implies that parcels of water that retain a disequilibrium between ocean and atmosphere gas concentrations, can still experience large density changes due to surface buoyancy forcing. This allows these water masses to participate in the overturning circulation and potentially be subducted to depth, limiting the parcel from future interaction with the atmosphere. This is of particular importance for analyses that use transit time distributions (TTDs) to infer

water mass pathways throughout the ocean [e.g., *Waugh et al*., 2006; *Peacock and Maltrud*, 2006]. These studies typically assume that water parcels instantaneously equilibrate with the atmospheric gas concentrations in determining surface initial conditions. This study suggests that additional information about surface residence times could influence these surface boundary conditions.

4.4. Limitations of the Study

This study provides new insight into the three-dimensional pathways of upwelling water masses, localized regions of outcropping, and mixed layer residence times in the Southern Ocean. However, the scope of the study is necessarily limited by a number of factors that may affect the robustness of the result. Firstly, the horizontal resolution of the OFES model is 1/10°, meaning that it does not resolve submesoscale features. Submesoscale features have been shown to be significant in enhancing vertical velocities as well as exchange across the base of the mixed layer [*Klein and Lapeyre*, 2009; *Thomas et al*., 2013]. These features are not represented in this model, nor are they parameterized. Observational evidence of the prevalence of submesoscale dynamics in the Southern Ocean has been limited, however, the region is preconditioned to be favorable to these types of flows due to the presence of eddying currents and filamentation, frequent storms and a long-term, down-front orientation of the wind stress with geostrophic fronts. One of the benefits of this study was the ability to use offline GCM data with a temporal resolution of three days. If a submesoscale-resolving model were to be used in place of OFES, the model output may need to be loaded with greater frequency, making the study significantly more computationally expensive.

As detailed in section 2, drifter motion in the mixed layer is represented by a random walk with a maximum velocity of 0.28 cm s^{-1}, consistent with estimates of vertical diffusivities within the mixed layer. The additional constraint is placed upon the drifters that they cannot vertically advect out of the mixed layer, in order to prevent the case where drifters continually oscillate across the base of the mixed layer. However, this may be a crude approximation to true mixed layer-interior exchange dynamics. For instance, active mixing layers may be decoupled from the total depth of the mixed layer for a number of reasons, including surface restratification by buoyancy or wind forcing [*Taylor and Ferrari*, 2010]. By forcing drifters to remain in the mixed layer until the boundary shoals or they horizontally advect across a strong gradient in mixed layer depth, we may be artificially enhancing the residence time of the mixed layer. We note that both localized convective events and advection by enhanced vertical velocities at the ocean submesoscale are not resolved by the OFES model. These have the potential to make a significant contribution to the total mixed layer-interior exchange, but observations of these processes in the Southern Ocean are limited. For this reason we have decided not to try and represent their effects by parameterizations, as in *Omand et al*. [2015].

We have also neglected interior diapycnal mixing in our advective scheme, constraining the drifters to move along isopycnals outside of the mixed layer. Previous observations of the Southern Ocean have shown diapycnal mixing to be large in localized regions of the ACC, especially near shallow/rough topography [*Naveira Garabato et al*., 2004; *LaCasce et al*., 2014], such as the outcropping regions identified here. However, throughout the bulk of the Southern Ocean, the approximation of isopycnal movement is a sound one, and the deep mixed layers near significant topographic features in the model may imitate the diapycnal mixing in these regions.

Lastly, this study was intentionally broad in its scope, attempting to sample the entire Southern Ocean and identify specific outcropping hotspots. Now that such regions have been identified, further work can be done targeting the source regions of specific water masses from each ocean basin. Site- or basin-specific sampling could be probed with numerical models that have a higher resolution than was employed in this study.

5. Conclusions

This study employs an eddy-resolving OFES GCM to explore the Lagrangian pathways of upwelling in the Southern Ocean. Virtual drifters were deployed across the Southern Ocean in two seasons, allowing us to examine both spatial and temporal variability of outcropping.

Specific sites stand out as "hotspots" where the majority of waters upwell into the mixed layer. The locations of these hotspots, in the lee of Kerguelen and Campbell Plateaus, around the East Pacific Rise, and through Drake Passage, suggest not only geographic localization but topographic control of upwelling. The use of virtual drifters allows for analysis at finer scales than previous methods that have studied outcropping and

subduction in the region, e.g., *Sallée et al*. [2010]; *Gebbie and Huybers* [2011]. This allows for the identification of smaller-scale features and variability, although the broad patterns are consistent with these previous result. The confirmation of strong topographic control on mixed layer ventilation is an important result with respect to longer-scale climate variability, in that this feature is likely less susceptible to temporal changes and might focus future observational efforts or paleoceanographic studies.

Several scales of variability are highlighted in the patterns of outcropping in the Southern Ocean. The intrabasin contrast reflects a wavenumber 1 pattern, with very little outcropping occurring in the Atlantic and most drifters upwelling in the Pacific basin. However, there are many smaller-scale variations as well. Large bathymetric features show strong and abrupt changes in outcropping frequency moving from the upstream to downstream sides. There is also potentially mesoscale variability due to the generation of deeper mixed layers in the lee of strong topography. As discussed in section 4.4, one of the limitations of the study is the resolution of the chosen GCM, limiting our ability to assess the impact of submesoscale processes on outcropping frequency and surface residence times.

We have also demonstrated that the mixed layer residence time is short, as compared to the duration of the trajectories. Drifters may outcrop into the mixed layer multiple times during their life span, however, each outcropping event is associated with a residence time on the order of one month; residence times greater than a year are observed infrequently. The cumulative residence times experienced by the drifters are similarly short, although a small subset of drifters spent between 1 and 3 years in the mixed layer over the 4 year simulation. When examined in conjunction with studies of air-sea equilibration timescales [e.g., *Jones et al*., 2014], this suggests that mixed layer residence time is a significant hindrance to achieving air-sea equilibrium of certain gases, such as CO_2 (typical residence time of 6–12 months) and $^{14}CO_2$ (typical residence time of order 10 years), in the Southern Ocean.

This study suggests that the Lagrangian time history of water parcels in the Southern Ocean may impact interior tracer distributions. We have not assessed the impact of these outcropping frequencies on the overturning circulation, as modulated by surface buoyancy forcing, but we note that assessments of the strength of this modification typically apply time-averaged or climatological distributions of mixed layer depths as well as heat and freshwater forcing. This study points to the need, in future work, to assess the temporal correlation of these properties and their impact on global water mass transformation rates.

Acknowledgments

We thank Jess Adkins, Matt Mazloff, and Jean-Baptiste Sallée for helpful discussions during this work. Erik van Sebille and one anonymous reviewer provided insightful comments that were invaluable in improving this manuscript. AFT gratefully acknowledges support from the National Science Foundation (OCE-1235488). GAV thanks the Vanoni Fellowship for supporting this work. The model output used are listed in the references and available from JAMSTEC at http://www.jamstec.go.jp/esc/research/AtmOcn/product/ofes.html. The Argo-derived mixed layer depth data are available at http://apdrc.soest.hawaii.edu/datadoc/mld.php.

References

Bishop, S. P., P. R. Gent, F. O. Bryan, A. F. Thompson, M. C. Long, and R. P. Abernathey (2016), Southern ocean overturning compensation in an eddy-resolving climate simulation, *J. Phys. Oceanogr.*, *46*, 1575–1592.

Bopp, L., M. Lévy, L. Resplandy, and J.-B. Sallée (2015), Pathways of anthropogenic carbon subduction in the global ocean, *Geophys. Res. Lett.*, *42*, 6416–6423, doi:10.1002/2015GL065073.

Broecker, W. S., et al. (1998), How much deep water is formed in the southern ocean?, *J. Geophys. Res.*, *103*, 15,833–15,843.

Cerovečki, I., L. D. Talley, and M. R. Mazloff (2011), A comparison of southern ocean air-sea buoyancy fluxes from an ocean state estimate with five other products, *J. Clim.*, *24*, 6283–6306.

Davis, R. E., P. D. Killworth, and J. R. Blundell (1996), Comparison of autonomous Lagrangian circulation explorer and fine resolution antarctic model results in the South Atlantic, *J. Geophys. Res.*, *101*, 855–884.

de Boyer Montégut, C., G. Madec, A. S. Fischer, A. Lazar, and D. Iudicone (2004), Mixed layer depth over the global ocean: An examination of profile data and a profile-based climatology, *J. Geophys. Res.*, *109*, C12003, doi:10.1029/2004JC002378.

Dong, S., J. Sprintall, S. T. Gille, and L. D. Talley (2008), Southern Ocean mixed-layer depth from argo float profiles, *J. Geophys. Res.*, *113*, C06013, doi:10.1029/2006JC004051.

Donners, J., S. S. Drijfhout, and W. Hazeleger (2005), Water mass transformation and subduction in the South Atlantic, *J. Phys. Oceanogr.*, *35*, 1841.

Dufour, C. O., J. Le Sommer, J. D. Zika, M. Gehlen, J. C. Orr, P. Mathiot, and B. Barnier (2015), Standing and transient eddies in the response of the southern ocean meridional overturning to the southern annular mode, *J. Clim.*, *25*, 6958–6974.

Ferrari, R., M. F. Jansen, J. F. Adkins, A. Burke, A. L. Stewart, and A. F. Thompson (2014), Antarctic sea ice control on ocean circulation in present and glacial climates, *Proc. Natl. Acad. Sci. U. S. A.*, *111*, 8753–8758.

Friocourt, Y., S. Drijfhout, B. Blanke, and S. Speich (2005), Water mass export from drake passage to the Atlantic, Indian, and Pacific oceans: A Lagrangian model analysis, *J. Phys. Oceanogr.*, *35*, 1206–1222.

Gary, S. F., M. S. Lozier, A. Biastoch, and C. W. B'oning (2012), Reconciling tracer and float observations of the export pathways of Labrador Sea Water, *Geophys. Res. Lett.*, *39*, L24606, doi:10.1029/2012GL053978.

Gebbie, G., and P. Huybers (2011), How is the ocean filled?, *Geophys. Res. Lett.*, *38*, L06604, doi:10.1029/2011GL046769.

Hägeli, P., D. G. Steyn, and K. B. Strawbridge (2000), Spatial and temporal variability of mixed-layer depth and entrainment zone thickness, *Boundary Layer Meteorol.*, *97*, 47–71.

Iudicone, D., G. Madec, and T. J. McDougall (2008), Water-mass transformations in a neutral density framework and the key role of light penetration, *J. Phys. Oceanogr.*, *38*, 1357–1376.

Jones, C. S., and P. Cessi (2016), Interbasin transport of the meridional overturning circulation, *J. Phys. Oceanogr.*, *46*, 1157–1169.

Jones, D. C., T. Ito, Y. Takano, and W.-C. Hsu (2014), Spatial and seasonal variability of the air-sea equilibration timescale of carbon dioxide, *Global Biogeochem. Cycles*, *28*, 1163–1178, doi:10.1002/2014GB004813.
Klein, P., and G. Lapeyre (2009), The oceanic vertical pump induced by mesoscale and submesoscale turbulence, *Annu. Rev. Mar. Sci.*, *1*, 351–375.
Kwon, Y. O., J. J. Park, S. F. Gary, and M. S. Lozier (2015), Year-to-year reoutcropping of eighteen degree water in an eddy-resolving ocean simulation, *J. Phys. Oceanogr.*, *45*, 1189–1204.
LaCasce, J. H., R. Ferrari, J. Marshall, R. Tulloch, D. Balwada, and K. Speer (2014), Float-derived isopycnal diffusivities in the dimes experiment, *J. Phys. Oceanogr.*, *44*, 764–780.
Large, W. G., J. C. McWilliams, and S. C. Doney (1994), Oceanic vertical mixing: A review and a model with a nonlocal boundary layer parameterization, *Rev. Geophys.*, *32*, 363–403.
Le Quéré, C., et al. (2009), Trends in the sources and sinks of carbon dioxide, *Nat. Geosci.*, *2*(12), 831–836.
Lévy, M., L. Bopp, P. Karleskind, L. Resplandy, C. Ethe, and F. Pinsard (2013), Physical pathways for carbon transfers between the surface mixed layer and the ocean interior, *Global Biogeochem. Cycles*, *27*, 1001–1012, doi:10.1002/gbc.20092.
Marshall, J., and T. Radko (2003), Residual-mean solutions for the antarctic circumpolar current and its associated overturning circulation, *J. Phys. Oceanogr.*, *33*, 2341–2354.
Marshall, J., and K. Speer (2012), Closure of the meridional overturning circulation through southern ocean upwelling, *Nat. Geosci.*, *5*, 171–180.
Masumoto, Y., et al. (2004), A fifty-year eddy-resolving simulation of the world ocean–Preliminary outcomes of OFES (OGCM for the earth simulator), *J. Earth Simulator*, *1*, 35–56.
Matear, R. (2001), Effects of numerical advection schemes and eddy parameterizations on ocean ventilation and oceanic anthropogenic co_2 uptake, *Ocean Modell.*, *3*, 217–248.
McPhee, M. G., and D. G. Martinson (1994), Turbulent mixing under drifting pack ice in the Weddell sea, *Science*, *263*(5144), 218–221.
Naveira Garabato, A. C., K. L. Polzin, B. A. King, K. J. Heywood, and M. Visbeck (2004), Widespread intense turbulent mixing in the southern ocean, *Science*, *303*, 210–213.
Naveira Garabato, A. C., K. L. Polzin, R. Ferrari, J. D. Zika, and A. Forryan (2016), A microscale view of mixing and overturning across the antarctic circumpolar current, *J. Phys. Oceanogr.*, *46*, 233–254.
Newsom, E. R., C. M. Bitz, F. O. Bryan, R. Abernathey, and P. R. Gent (2016), Southern ocean deep circulation and heat uptake in a high-resolution climate model, *J. Clim.*, *29*, 2597–2619.
Omand, M. M., E. A. D'Asaro, C. M. Lee, M. J. Perry, N. Briggs, I. Cetini, and A. Mahadevan (2015), Eddy-driven subduction exports particulate organic carbon from the spring bloom, *Science*, *348*(6231), 222–225.
Orsi, A. H., T. Whitworth, and W. D. Nowlin, Jr. (1995), On the meridional extent and fronts of the Antarctic Circumpolar Current, *Deep Sea Res., Part I*, *42*(5), 641–673.
Peacock, S., and M. Maltrud (2006), Transit-time distributions in a global ocean model, *J. Phys. Oceanogr.*, *36*, 474–495.
Piñones, A., E. E. Hofmann, M. S. Dinniman, and J. M. Klinck (2011), Lagrangian simulation of transport pathways and residence times along the western Antarctic Peninsula, *Deep Sea Res., Part II*, *58*(13–16), 1524–1539.
Rintoul, S. R. (2013), Large-scale ocean circulation: Deep circulation and meridional overturning, in *Earth System Monitoring*, edited by J. Orcutt, pp. 199–232, Springer, N. Y.
Sallée, J.-B., K. Speer, S. R. Rintoul, and S. Wijffels (2010), Southern ocean thermocline ventilation, *J. Phys. Oceanogr.*, *40*, 509–529.
Sallée, J.-B., R. J. Matear, S. R. Rintoul, and A. Lenton (2012), Localized subduction of anthropogenic carbon dioxide in the southern hemisphere oceans, *Nat. Geosci.*, *26*(1), 80–97.
Sarmiento, J. L., J. C. Orr, and U. Siegenthaler (1992), A perturbation simulation of co_2 uptake in an ocean general circulation model, *J. Geophys. Res.*, *97*, 3621–3645.
Sheen, K. L., et al. (2013), Rates and mechanisms of turbulent dissipation and mixing in the southern ocean: Results from the diapycnal and isopycnal mixing experiment in the southern ocean (dimes), *J. Geophys. Res. Oceans*, *118*, 2774–2792, doi:10.1002/jgrc.20217.
Smethie, W. M., Jr., and R. A. Fine (2001), Rates of North Atlantic deep water formation calculated from chlorofluorocarbon inventories, *Deep Sea Res., Part I*, *48*, 189–215.
Talley, L. D. (2013), Closure of the global overturning circulation through the Indian, Pacific, and Southern oceans: Schematics and transports, *Oceanography*, *26*(1), 80–97.
Tamsitt, V., L. D. Talley, M. R. Mazloff, and I. Cerovečki (2015), Zonal variations in the southern ocean heat budget, *J. Clim.*, doi:10.1175/JCLI-D-15-0630.1, in press.
Taylor, J. R., and R. Ferrari (2010), Buoyancy and wind-driven convection at mixed layer density fronts, *J. Phys. Oceanogr.*, *40*, 1222–1242.
Thomas, L. N., J. R. Taylor, R. Ferrari, and T. M. Joyce (2013), Symmetric instability in the gulf stream, *Deep Sea Res., Part II*, *91*, 96–110.
Thompson, A. F., and K. J. Richards (2011), Low frequency variability of southern ocean jets, *J. Geophys. Res.*, *116*, C09022, doi:10.1029/2010JC006749.
Thompson, A. F., and J.-B. Sallée (2012), Jets and topography: Jet transitions and the impact on transport into the Antarctic circumpolar current, *J. Phys. Oceanogr.*, *42*, 956–972.
Thompson, A. F., K. J. Heywood, and S. Schmidtko (2014), Eddy transport as a key component of the Antarctic overturning circulation, *Nat. Geosci.*, *7*, 879–884.
Thompson, A. F., A. L. Stewart, and T. Bischoff (2015), A multi-basin residual-mean model for the global overturning circulation, *J. Phys. Oceanogr.*, doi:10.1175/JPOD-15-0204.1, in press.
van Sebille, E., P. J. van Leeuwen, A. Biastoch, C. N. Barron, and W. P. M. de Ruijter (2009), Lagrangian validation of numerical drifter trajectories using drifting buoys: Application to the Agulhas system, *Ocean Modell.*, *29*(4), 269–276.
van Sebille, E., M. H. England, J. D. Zika, and B. M. Sloyan (2012), Tasman leakage in a fine-resolution ocean model, *Geophys. Res. Lett.*, *39*, L06601, doi:10.1029/2012GL051004.
van Sebille, E., P. Spence, M. R. Mazloff, M. H. England, S. R. Rintoul, and O. E. Saenko (2013), Abyssal connections of Antarctic Bottom Water in a Southern Ocean State Estimate, *Geophys. Res. Lett.*, *40*, 2177–2182, doi:10.1002/grl.50483.
Waugh, D. W., T. M. Hall, B. I. McNeil, R. Key, and R. J. Matear (2006), Anthropogenic CO_2 in the oceans estimated using transit time distributions, *Tellus, Ser. B*, *58*(5), 376–389.
Weijer, W., W. De Ruijter, A. Sterl, and S. Drijfhout (2002), Response of the Atlantic overturning circulation to South Atlantic sources of buoyancy, *Global Planet. Change*, *34*, 293–311.